International Journal of Fracture **84:** 203–228, 1997.

Quasi-statically growing crack-tip fields in elastic perfectly plastic pressure-sensitive materials under plane strain conditions

W.J. CHANG, M. KIM and J. PAN
Mechanical Engineering and Applied Mechanics, The University of Michigan, Ann Arbor, MI 48109, USA
e-mail: jwo@engin.umich.edu.

Received 25 October 1996; accepted in revised form 28 February 1997

Abstract. Quasi-statically growing crack-tip fields in elastic perfectly plastic pressure-sensitive materials under plane strain conditions are investigated in this paper. The materials are assumed to follow the Drucker–Prager yield criterion and the normality flow rule. The asymptotic mode I crack-tip fields are assumed to follow the five-sector assembly of Drugan et al. (1982) for Mises materials. The crack-tip sectors, in turns, from the front of the crack tip are a constant stress sector, a centered fan sector, a non-singular plastic sector, an elastic sector and finally a trailing non-singular plastic sector bordering the crack face. The results of the asymptotic analysis show that as the pressure sensitivity increases, the plastic deformation shifts to the front of the tip, the angular span of the elastic unloading sector increases, and the angular span of the trailing non-singular plastic sector bordering the crack surface decreases. As the pressure sensitivity increases to about 0.6, the angular span of the trailing non-singular plastic sector almost vanishes. The effects of the border conditions between the centered fan sector and the first non-singular plastic sector on the solutions of the crack-tip fields for both Mises and pressure-sensitive materials are investigated in details.

Key words: asymptotic analyses, growing cracks, pressure sensitivity, perfectly plastic materials

1. Introduction

In the classical metal plasticity theory, it is assumed that hydrostatic pressure has no effect on material plastic deformation, and plastic dilatancy is neglected. However, for many materials, such as soils, concrete, rocks and silicate glasses, macroscopic pressure-sensitive yielding and plastic volumetric deformation are exhibited. Toughened plastics also show apparent pressure-sensitive yielding and plastic volumetric deformation, for example, see [1, 2, 3, 4]. Pressure-sensitive phase transformation (or yielding) is also observed in zirconia-containing transformation toughened ceramics, for example, see [5, 6, 7]. It is considered that the pressure-sensitive yielding occurs from basic flow mechanism, cavitation and craze formation in some polymers and from phase transformation and microcracking in some ceramics.

The available asymptotic near-tip fields for stationary cracks in highly pressure-sensitive materials show different characteristics from those in pressure-insensitive Mises materials. Li and Pan [9, 10] studied the effects of pressure-sensitive yielding on asymptotic crack-tip fields based on the Drucker–Prager yield criterion [8] for power-law hardening deformation plasticity materials and perfectly plastic materials under mode I plane strain and plane stress conditions. They found that asymptotic HRR-type crack-tip fields (Hutchinson [11, 12]; Rice and Rosengren [13]) do exist for pressure-sensitive power-law hardening materials. The results of Li and Pan [9, 10] show that pressure sensitivity can lower the mean stress and the effective stress directly ahead of the crack tip. Further investigations on characterization of asymptotic crack-tip fields based on the Drucker–Prager yield criterion can be found in Yuan and Lin [14] and Yuan [15].

The crack-tip field of a stationary crack in perfectly plastic Mises materials under mode I plane strain conditions can be described by the fully-yielded Prandtl field. However, when the Prandtl field is directly applied to a moving crack, negative plastic dissipation occurs along the border between the centered fan sector and the trailing constant stress sector. Studies of the crack-tip fields for moving cracks in elastic perfectly plastic Mises materials show that there are indeed additional restrictions for moving cracks [16, 17, 18, 19].

Works contributed to the asymptotic solutions of mode I near-tip fields of quasi-statically growing cracks in elastic perfectly plastic materials under plane strain conditions are briefly summarized in the following. Slepyan [20] first obtained the solutions for Tresca materials. Gao [21] later independently developed the solution for Mises materials with Poisson's ratio ν equal to $\frac{1}{2}$. Rice et al. [22] included an elastic unloading zone between the centered fan sector and the trailing constant stress sector instead of the fully-yielded Prandtl field which should not be adopted due to its negative plastic dissipation for a growing crack. Subsequently, Rice [23] conducted more rigorous studies of anti-plane strain, plane strain and plane stress asymptotic crack-tip fields for materials following a general form of yield criteria and the normality flow rule.

Rice [23] pointed out an error in the solution of Rice et al. [22] for $\nu < \frac{1}{2}$. Drugan et al. [24] corrected the error and introduced an asymptotic growing crack-tip field with two non-singular plastic sectors for $\nu < \frac{1}{2}$. The results of their study showed a general agreement with the finite element solutions of Sham [25]. However, Hwang and Luo [26] later discovered negative plastic dissipation in a part of the first non-singular plastic sector in the solution of Drugan et al. [24] for $\nu < \frac{1}{2}$. Hwang and Luo [26] adopted a border condition, from Gao and Hwang [17], between the first non-singular plastic sector and the elastic sector and then obtained the asymptotic crack-tip fields. Their results showed that the asymptotic structure of the stress field for $\nu < \frac{1}{2}$ tends to that for $\nu = \frac{1}{2}$ when ν approaches to $\frac{1}{2}$. To extend the analytical studies to large-scale and general yielding conditions, Drugan and Chen [27] further assumed a curved asymptotic boundary between the front constant stress sector and the centered fan sector and obtained the 'm-family' analytical solutions for Mises materials with $\nu = 1/2$. In Chen and Drugan [28], the 'm-family' solutions are shown to compare well with the corresponding finite element solutions for finite geometries.

In contrast to the crack-tip fields for elastic perfectly plastic materials, Ponte Castañeda [29] investigated asymptotic crack-tip fields for quasi-statically growing cracks in Mises materials with linear hardening. He was able to obtain results for materials with very low strain hardening. However, some characteristics of his results are not in good agreement with those for elastic perfectly plastic materials as in Drugan et al. [24]. A similar approach was adopted in the work of Bigoni and Radi [30] for pressure-sensitive materials with linear hardening based on the Drucker–Prager yield criterion. The crack-tip fields of Bigoni and Radi [30] showed the similar trend of lower stresses ahead of the tip due to pressure sensitivity when compared with the asymptotic crack-tip fields of Li and Pan [9, 10] for stationary cracks in pressure-sensitive materials.

In this paper, the asymptotic crack-tip fields for quasi-statically growing cracks under plane strain conditions are constructed for pressure-sensitive materials based on the Drucker–Prager yield criterion. The assembly of the crack-tip sectors suggested by Drugan et al. [24] for Mises materials with $\nu < \frac{1}{2}$ is adopted for pressure-sensitive materials. We follow the framework established by Rice [23] to determine the stress and velocity fields in each crack-tip sector. The conditions along the border between the centered fan and the first non-singular plastic sector are examined in details. The crack-tip fields for various values of pressure sensitivity are

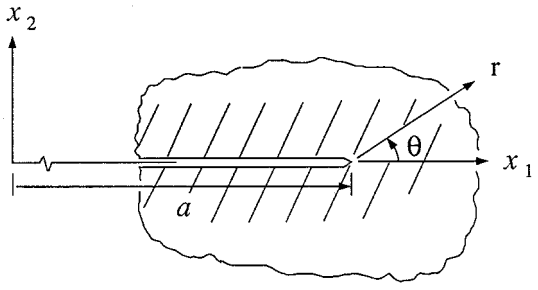

Figure 1. Cartesian coordinates x_1, x_2 and x_3 are fixed in the material; polar coordinates r and θ are centered at the tip and move with the tip as the crack grows.

obtained and the stresses ahead of the crack tip are compared with those of the fully-yielded crack-tip fields for stationary cracks.

2. Governing equations

Figure 1 shows a crack with a length a. In the figure, x_1 and x_2 represent the fixed Cartesian coordinates, and r and θ represent the polar coordinates centered at the growing crack tip. The crack is assumed to grow in the x_1 direction.

2.1. EQUILIBRIUM

The equilibrium equations are

$$\frac{\partial \sigma_{ij}}{\partial x_j} + f_i = 0, \tag{1}$$

where σ_{ij} represent the stress components and f_i are the components of the body force. The subscripts i, j and k have the range of 1 to 3 and the summation convention is adopted. If only the leading dominant terms are considered, the asymptotic form ($r \to 0$) of the in-plane equilibrium equations for growing cracks, in terms of the polar components of stresses, can be written as (see Rice [23] and Drugan [18])

$$\sigma_{rr} - \sigma_{\theta\theta} + \sigma'_{r\theta} = 0 \tag{2}$$

$$2\sigma_{r\theta} + \sigma'_{\theta\theta} = 0, \tag{3}$$

where $\sigma'_{r\theta}$ and $\sigma'_{\theta\theta}$ represent the derivatives of $\sigma_{r\theta}$ and $\sigma_{\theta\theta}$ with respect to θ as $r \to 0$. Under mode I plane strain conditions, a very useful relation which is also derived from the equilibrium equations (Rice [23]) is

$$\sigma'_{ij} H_{ij} = (\sigma'_{11} + \sigma'_{22}) H_{rr} + \sigma'_{33} H_{33}, \tag{4}$$

where σ'_{ij} represent the derivatives of σ_{ij} with respect to θ as $r \to 0$ and H_{ij} are the components of an arbitrary tensor.

2.2. CONSTITUTIVE RELATIONS

The components of the rate of deformation tensor, D_{ij}, are defined as

$$D_{ij} = \dot{\epsilon}_{ij} = \frac{1}{2}\left(\frac{\partial v_i}{\partial x_j} + \frac{\partial v_j}{\partial x_i}\right), \tag{5}$$

where ϵ_{ij} are the strain components, the dot represents the time derivative at a fixed material point, v_i are the velocity components of a particle and $v_i = \dot{u}_i$ where u_i are the displacement components. D_{ij} can be decomposed into an elastic part, D^e_{ij}, and a plastic part, D^p_{ij}:

$$D_{ij} = D^e_{ij} + D^p_{ij}. \tag{6}$$

Based on Hooke's law for elastic isotropic materials, the elastic part D^e_{ij} can be expressed as

$$D^e_{ij} = M_{ijkl}\dot{\sigma}_{kl}, \tag{7}$$

where

$$M_{ijkl} = \frac{1+\nu}{2E}(\delta_{ik}\delta_{jl} + \delta_{il}\delta_{jk}) - \frac{\nu}{E}\delta_{ij}\delta_{kl}. \tag{8}$$

Here, δ_{ij} is the Kronecker delta. The asymptotic form of the stress rates $\dot{\sigma}_{ij}$ is represented in Equation (14). In Equation (8), E is Young's modulus and ν is Poisson's ratio.

The pressure-sensitive Drucker–Prager yield criterion [8, 9, 10] is adopted here. The yield criterion is a linear combination of the mean stress σ_m ($= \sigma_{kk}/3$) and the effective stress σ_e ($= 3\,(s_{ij}s_{ij}/2)^{1/2}$ where $s_{ij} = \sigma_{ij} - \sigma_m\delta_{ij}$) as

$$\psi(\sigma_{ij}) = \sigma_e + \sqrt{3}\mu\sigma_m = \sigma_{ge} = \sigma_0. \tag{9}$$

In Equation (9), $\psi(\sigma_{ij})$ represents the yield function of σ_{ij}, and μ represents the pressure sensitivity of the material. Here μ is taken as a constant. For steels, the values of μ are quite small in the range from 0.014 to 0.064 (Spitzig et al. [31, 32]). For polymers, the values of μ are in the range from 0.1 to 0.25 (Kinloch and Young [33]). For phase transformation ceramics, Chen [34] reported that μ is 0.55 for Mg-PSZ and 0.77 for Ce-TZP. For Ce-TZP, μ can be as high as 0.93 (Yu and Shetty [7]). In Equation (9), σ_{ge} represents the generalized tensile effective stress. For perfectly plastic materials, σ_{ge} is taken as a constant σ_0.

The assumption of normality for plastic strain increments leads to

$$D^p_{ij} = \dot{\Lambda}\, P_{ij}, \tag{10}$$

where $\dot{\Lambda}$ is a proportionality factor and P_{ij} represent the components of the outward normal to the yield surface in the stress space. Here, for the Drucker–Prager yield criterion, P_{ij} are written as

$$P_{ij} \equiv \frac{\partial\psi(\sigma_{ij})}{\partial\sigma_{ij}} = \frac{3s_{ij}}{2\sigma_e} + \frac{\mu}{\sqrt{3}}\,\delta_{ij}\,. \tag{11}$$

Thus,

$$D_{ij} = M_{ijkl}\dot{\sigma}_{kl} + \dot{\Lambda}\, P_{ij}. \tag{12}$$

Note that in Equation (12) the material has been assumed to follow the normality flow rule. For transformation toughened ceramics, the experimental results suggested that the phase transformation strain increments follow the normality flow rule [6]. However, non-normality flow occurs in plastics, rocks and metals, see Drucker [2], Rudnicki and Rice [35] and Needleman and Rice [36]. Here we will concentrate on the crack-tip behavior for pressure-sensitive materials with normality flow.

The constitutive relation, Equation (12), involves the stress rates with respect to a fixed material point. Applying the chain rule to the stress rates $\dot{\sigma}_{ij}(r, \theta, t)$, we get

$$\dot{\sigma}_{ij} = \frac{\partial \sigma_{ij}}{\partial \theta}\dot{\theta} + \frac{\partial \sigma_{ij}}{\partial r}\dot{r} + \frac{\partial \sigma_{ij}}{\partial t}. \tag{13}$$

Here the rates of the crack-tip polar coordinates can be expressed by $\dot{\theta} = \dot{a}\sin\theta/r$ and $\dot{r} = -\dot{a}\cos\theta$. The asymptotic form of the stress rates then becomes (Rice [23])

$$\dot{\sigma}_{ij} = \sigma'_{ij}\dot{a}\sin\theta/r \tag{14}$$

by considering only the leading-order terms. Note that Equation (14) is valid only for the indices of the Cartesian coordinates (i, $j = 1, 2$). With the use of Equations (14) and (4), the elastic part of D_{ij} can be written as

$$D^e_{ij} = M_{ijkl}\dot{\sigma}_{kl} = [M_{ijrr}(\sigma'_{11} + \sigma'_{22}) + M_{ij33}\sigma'_{33}]\dot{a}\sin\theta/r. \tag{15}$$

3. Elastic sector

Rice [23] has derived the stress field and kinematically admissible velocity field in an elastic sector. The compatibility for plane problems gives

$$\frac{\partial^2 D_{22}}{\partial x_1^2} + \frac{\partial^2 D_{11}}{\partial x_2^2} = 2\frac{\partial^2 D_{12}}{\partial x_1 \partial x_2}. \tag{16}$$

The components of the rate of deformation tensor are assumed in the form

$$D_{ij} \sim \dot{a}F_{ij}(\theta)/r. \tag{17}$$

The velocity fields which satisfy the compatibility Equation (16) under the assumption of Equation (17) can have the form

$$v_1 = \dot{a}\,A_6\,\ln|r\sin\theta/R| - \dot{a}\int (F_{11}(\theta)/\sin\theta)\,\mathrm{d}\theta, \tag{18}$$

$$v_2 = \dot{a}\,A_7\,\ln|r\cos\theta/R| + \dot{a}\int (F_{22}(\theta)/\cos\theta)\,\mathrm{d}\theta. \tag{19}$$

Here, R is a length parameter, and A_6 and A_7 are constants. Also,

$$F_{11}(\theta) = (\cos^2\theta - \nu)(A_6\cos\theta + A_7\sin\theta)/(1-\nu), \tag{20}$$

$$F_{22}(\theta) = (\sin^2\theta - \nu)(A_6\cos\theta + A_7\sin\theta)/(1-\nu). \tag{21}$$

The stress components in the elastic sector are

$$\sigma_{11} = \frac{E}{4(1-\nu^2)}[4A_6 \ln|\sin\theta| + A_6\cos 2\theta + A_7(2\theta + 2\sin 2\theta) + A_8], \tag{22}$$

$$\sigma_{12} = \frac{E}{4(1-\nu^2)}\left[A_6(2\theta + \sin 2\theta) - A_7\cos 2\theta + A_9\right], \tag{23}$$

$$\sigma_{22} = \frac{E}{4(1-\nu^2)}\left[-A_6\cos 2\theta + A_7(2\theta - \sin 2\theta) + A_{10}\right], \tag{24}$$

$$\sigma_{33} = \nu(\sigma_{11} + \sigma_{22}) + A_{11}, \tag{25}$$

where A_8, A_9, A_{10}, and A_{11} are constants to be determined from the boundary conditions.

4. Singular plastic sector

For plastic sectors, Rice [23] derived a differential form of the yield condition near the tip as

$$P_{ij}\sigma'_{ij} = 0. \tag{26}$$

Equation (26) is obtained from the fact that the yield criterion is satisfied for all angles inside plastic sectors for perfectly plastic materials. Applying Equation (4) to Equation (26), Rice then gave the governing equation for plastic sectors as

$$(\sigma'_{11} + \sigma'_{22})P_{rr} + \sigma'_{33}P_{33} = 0. \tag{27}$$

Further, these plastic sectors are categorized into two different types: singular plastic sectors with $P_{33} = 0$ and non-singular plastic sectors with $P_{33} \neq 0$.

The singular plastic sectors have at least one singular in-plane plastic strain component. For singular plastic sectors with $P_{33} = 0$ as $r \to 0$, Equation (27) becomes

$$(\sigma'_{11} + \sigma'_{22})P_{rr} = 0. \tag{28}$$

4.1. Constant stress sector

From the governing Equation (28) for singular plastic sectors, when $\sigma'_{11} + \sigma'_{22} = 0$, all the Cartesian stress components are constants in this type of sectors. The velocity field has the same form as that of the elastic sector under the assumption of Equation (17). But the constants A_6 and A_7 and $F_{ij}(\theta)$ are different such that

$$F_{11}(\theta) = \frac{r}{\dot{a}}\dot{\Lambda}P_{11} \tag{29}$$

$$F_{22}(\theta) = \frac{r}{\dot{a}}\dot{\Lambda}P_{22}, \tag{30}$$

and A_6 and A_7 are replaced by two other constants, C_1 and C_2, respectively.

4.2. Centered fan sector

When $P_{rr} = 0$, closed-form solutions for crack-tip stresses have been derived in Kim and Pan [37]. The solutions will not be repeated here. In order to find the kinematically admissible velocity fields, we multiply $r\,\partial\sigma_{ij}/\partial\theta$ to both sides of Equation (12)

$$r\,\frac{\partial\sigma_{ij}}{\partial\theta}D_{ij} = r\,\frac{\partial\sigma_{ij}}{\partial\theta}\left(M_{ijkl}\dot{\sigma}_{kl} + \dot{\Lambda}\,P_{ij}\right). \tag{31}$$

Here, $r(\partial\sigma_{ij}/\partial\theta)\dot{\Lambda}P_{ij}$ is zero for both elastic and plastic sectors because in elastic sectors $\dot{\Lambda} = 0$ and in plastic sectors $\sigma'_{ij}\,P_{ij} = 0$ (Equation (26)). With the use of Equation (4), $D_{rr} = \partial v_r/\partial r$ and $D_{33} = 0$, Equation (31) becomes

$$r\,\frac{\partial\, v_r}{\partial r} = \left[\sigma'_{11} + \sigma'_{22} - 2\,\nu\,\sigma'_{33} + \frac{(\sigma'_{33})^2}{\sigma'_{11} + \sigma'_{22}}\right]\,\frac{\dot{a}}{E}\,\sin\theta, \tag{32}$$

as $r \to 0$.

Integrating Equation (32) gives the velocity component v_r in the centered fan sector as

$$v_r = Y(\theta)\,\frac{\dot{a}}{E}\ln|R/r| + \frac{\partial f(\theta,t)}{\partial\theta}, \tag{33}$$

where

$$Y(\theta) = -\sin\theta\left[\sigma'_{11} + \sigma'_{22} - 2\nu\sigma'_{33} + \frac{(\sigma'_{33})^2}{\sigma'_{11} + \sigma'_{22}}\right] \tag{34}$$

and $f(\theta,t)$ is a function of integration. In order to find v_θ, the components $D_{\theta\theta}$ and $D_{r\theta}$ are obtained from using Equations (12) and (15) and by noting that $M_{\theta\theta rr} = M_{\theta\theta 33} = -\nu/E$ and $M_{r\theta rr} = M_{r\theta 33} = 0$ as

$$D_{\theta\theta} \;=\; -\frac{\nu}{E}\sigma'_{kk}\frac{\dot{a}}{r}\sin\theta + \dot{\Lambda}P_{\theta\theta} \tag{35}$$

$$D_{r\theta} \;=\; \dot{\Lambda}P_{r\theta}. \tag{36}$$

Also, the relations of $D_{r\theta}$ and $D_{\theta\theta}$ to v_r and v_θ from Equation (5) are

$$D_{\theta\theta} \;=\; \frac{1}{r}\frac{\partial v_\theta}{\partial\theta} + \frac{v_r}{r} \tag{37}$$

$$D_{r\theta} \;=\; \frac{1}{2}\left(\frac{1}{r}\frac{\partial v_r}{\partial\theta} + \frac{\partial v_\theta}{\partial r} - \frac{v_\theta}{r}\right). \tag{38}$$

After combining Equations (35), (37) and (33) and integrating the result over θ, we get an expression for v_θ as

$$\begin{aligned} v_\theta \;=\; & -\frac{\dot{a}}{E}\int_{\theta_0}^{\theta}\nu\sigma'_{kk}\sin\theta\;\mathrm{d}\theta + \int_{\theta_0}^{\theta} r\dot{\Lambda}P_{\theta\theta}\;\mathrm{d}\theta \\ & -\frac{\dot{a}}{E}\ln|R/r|\int_{\theta_0}^{\theta} Y(\theta)\;\mathrm{d}\theta - f(\theta,t) + g(r,t), \end{aligned} \tag{39}$$

where θ_0 is the angle where the centered fan begins and $g(r,t)$ is a function of integration. Here $g(r,t)$ is considered as the contribution from rigid body motion. Note that in Equation (39) the dependence of $\dot{\Lambda}$ on r and θ is still not known.

In order to understand the functional form of $\dot{\Lambda}$, we combine Equations (36) and (38) with the velocities v_r and v_θ from Equations (33) and (39) and we have

$$\dot{\Lambda}P_{r\theta} \;=\; \frac{\dot{a}}{2E}\frac{1}{r}\ln|R/r|\left(\frac{dY(\theta)}{\mathrm{d}\theta} + \int_{\theta_0}^{\theta} Y(\theta)\;\mathrm{d}\theta\right) + \frac{\dot{a}}{2E}\frac{1}{r}\int_{\theta_0}^{\theta}\nu\sigma'_{kk}\sin\theta\;\mathrm{d}\theta$$

$$+\frac{\dot{a}}{2E}\frac{1}{r}\int_{\theta_0}^{\theta} Y(\theta)\ \mathrm{d}\theta + \frac{1}{2}\int_{\theta_0}^{\theta}\left(r\frac{\partial\dot{\Lambda}}{\partial r}\right)P_{\theta\theta}\ \mathrm{d}\theta$$

$$+\frac{1}{2r}\left[\frac{\partial^2 f(\theta,t)}{\partial\theta^2}+f(\theta,t)\right]+\left[\frac{\partial g(r,t)}{\partial r}-\frac{g(r,t)}{r}\right]. \tag{40}$$

We assume the functional form of $\dot{\Lambda}$ to satisfy Equation (40) as

$$\dot{\Lambda}\to X(\theta)\frac{1}{r}\ln(R/r)\frac{\dot{a}}{E}+W(\theta)\frac{\dot{a}}{r}+Z(\theta)\frac{1}{r}\quad\text{as } r\to 0. \tag{41}$$

Here $X(\theta)$, $W(\theta)$, and $Z(\theta)$ are functions of θ. Now we substitute Equation (41) into (40) and compare the coefficients of the most singular terms with $1/r\ln|R/r|$. Then we obtain the governing equation for $X(\theta)$ as

$$P_{r\theta}X(\theta)=\frac{1}{2}\left\{\frac{\mathrm{d}Y(\theta)}{\mathrm{d}\theta}+\int_{\theta_0}^{\theta}Y(\theta)\ \mathrm{d}\theta\right\}-\frac{1}{2}\int_{\theta_0}^{\theta}P_{\theta\theta}X(\theta)\ \mathrm{d}\theta. \tag{42}$$

For convenience of numerical calculation, we rewrite Equation (42) in the form of differential equation as

$$P_{r\theta}X'(\theta)+(P'_{r\theta}+\tfrac{1}{2}P_{\theta\theta})X(\theta)=\frac{1}{2}\left(\frac{\mathrm{d}^2Y(\theta)}{\mathrm{d}\theta^2}+Y(\theta)\right) \tag{43}$$

with the boundary condition

$$X(\theta_0)=\left.\frac{1}{2P_{r\theta}}\frac{\mathrm{d}Y(\theta)}{\mathrm{d}\theta}\right|_{\theta=\theta_0}. \tag{44}$$

In summary, if only the most singular terms are considered for $\dot{a}\neq 0$, the velocity components in the centered fan sector become

$$v_r = Y(\theta)\frac{\dot{a}}{E}\ln|R/r| \tag{45}$$

$$v_\theta = -\frac{\dot{a}}{E}\ln|R/r|\int_{\theta_0}^{\theta}[Y(\theta)-P_{\theta\theta}X(\theta)]\ \mathrm{d}\theta, \tag{46}$$

as $r\to 0$. Note that $Y(\theta)$ and $P_{\theta\theta}$ can be obtained from the closed-form solution of Kim and Pan [37]. We need to determine $X(\theta)$ numerically from integrating Equation (43) with the boundary condition (44).

Let us check the velocity field of the centered fan sector in Equations (45) and (46) for the limit case of $\mu=0$. For Mises materials ($\mu=0$), $\sigma'_{33}=(\sigma'_{11}+\sigma'_{22})/2=-2\tau_0$ where τ_0 is the shear yield stress ($\tau_0=\sigma_0/\sqrt{3}$). From Equation (34) we can have

$$Y(\theta)=(5-4\nu)\tau_0\sin\theta. \tag{47}$$

Also, since $P_{rr}=P_{33}=0$ in the centered fan sector, we have $P_{\theta\theta}=0$ due to plastic incompressibility for $\mu=0$. Therefore, with the centered fan beginning at $\theta=45^\circ$ for Mises materials, Equations (45) and (46) are reduced to

$$v_r = (5-4\nu)(\tau_0/E)\dot{a}\sin\theta\ln|R/r| \tag{48}$$

$$v_\theta = -(5-4\nu)(\tau_0/E)\dot{a}\left[1/\sqrt{2}-\cos\theta\right]\ln|R/r|, \tag{49}$$

which are in agreement with those of Rice [23] and Drugan et al. [24] for Mises materials.

5. Non-singular plastic sector

We now consider non-singular plastic sectors where the material deforms plastically but $P_{33} \neq 0$ in Equation (27) as $r \to 0$. From Equations (12) and (15), the plane strain conditions for such a sector give

$$D_{33} = 0 = \frac{\sigma'_{33} - \nu(\sigma'_{11} + \sigma'_{22})}{E} \frac{\dot{a}}{r} \sin\theta + \dot{\Lambda} P_{33}, \tag{50}$$

or,

$$\dot{\Lambda} = -\frac{\sigma'_{33} - \nu(\sigma'_{11} + \sigma'_{22})}{E P_{33}} \frac{\dot{a}}{r} \sin\theta. \tag{51}$$

The equilibrium equations, Equations (2) and (3), can be rewritten as

$$\sigma'_{r\theta} = 2\,(\sigma_{\theta\theta} - \sigma) \tag{52}$$

$$\sigma'_{\theta\theta} = -2\,\sigma_{r\theta}, \tag{53}$$

where $\sigma = (\sigma_{rr} + \sigma_{\theta\theta})/2$. As in Rice [23], combining the compatibility equation and the differential form of the yield condition gives

$$\left[\left(1 + \nu\frac{P_{rr}}{P_{33}}\right)(\sigma'_{rr} + \sigma'_{\theta\theta}) - \left(\nu + \frac{P_{rr}}{P_{33}}\right)\sigma'_{33}\right] \sin\theta = E\,(A_1 \cos\theta + A_2 \sin\theta), \tag{54}$$

where A_1 and A_2 are constants to be determined from the velocity fields. The differential yield condition (27) can be rewritten as

$$(\sigma'_{rr} + \sigma'_{\theta\theta})P_{rr} + \sigma'_{33}P_{33} = 0. \tag{55}$$

Equation (55) can be further rewritten as

$$\sigma'_{33} = -2\sigma' \left(\frac{P_{rr}}{P_{33}}\right). \tag{56}$$

With the use of Equation (56), Equation (54) can also be rewritten as

$$\sigma' = \frac{E(A_1 \cos\theta/\sin\theta + A_2)}{2\{1 + 2\nu(P_{rr}/P_{33}) + (P_{rr}/P_{33})^2\}}. \tag{57}$$

Equations (52), (53), (56), and (57) define the stress field in the non-singular plastic sector. Under the same assumption of Equation (17), the velocity field in this sector can be expressed by Equations (18) and (19) (Rice [23]) with different constants and $F_{ij}(\theta)$. The constants A_6 and A_7 in Equations (18) and (19) should be replaced by A_1 and A_2, respectively, for the non-singular plastic sector. But the closed-form solutions of $F_{ij}(\theta)$ cannot be obtained because the governing equations for the stress field in the non-singular plastic sector cannot be solved analytically unless $A_1 = A_2 = 0$ in Equation (54), which gives the trivial solution of a constant stress state.

6. The assembly of sectors

The assembly of the quasi-statically growing crack-tip fields for elastically compressible ($\nu < 1/2$) Mises materials suggested by Drugan et al. [24] is adopted here and shown in

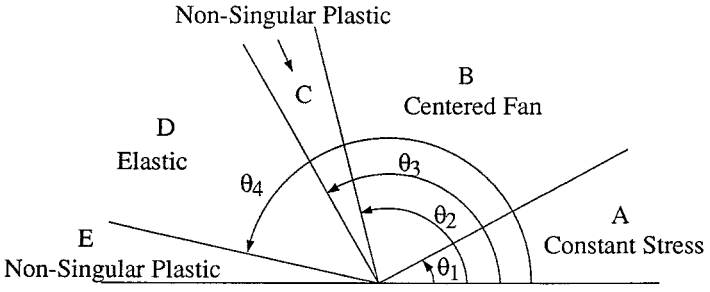

Figure 2. The assembly of crack-tip sectors for quasi-statically growing cracks.

Figure 2. The crack-tip sectors, in turns, from the front of the crack tip are a constant stress sector (sector A), a centered fan sector (sector B), a non-singular plastic sector (sector C), an elastic sector (sector D), and another non-singular plastic sector (sector E) bordering the crack surface. For Mises materials with $\nu \neq 1/2$, the five-sector assembly in Figure 2 has been numerically illustrated to approach to a four-sector assembly for $\nu = 1/2$ when ν increases to $\frac{1}{2}$ [26]. When $\mu = 0$ and $\nu = \frac{1}{2}$, the leading non-singular plastic sector (sector C) shrinks to a line, and the trailing non-singular plastic sector (sector E) becomes a constant stress sector [26].

The symmetry of mode I crack-tip fields requires

$$\sigma_{r\theta} = 0 \quad \text{and} \quad v_\theta = 0 \quad \text{at } \theta = 0^\circ. \tag{58}$$

The traction along the border between two sectors must be continuous. This gives the continuity of $\sigma_{\theta\theta}$ and $\sigma_{r\theta}$ along the border. The crack surface (at $\theta = 180^\circ$) should be traction-free. Therefore,

$$\sigma_{\theta\theta} = \sigma_{r\theta} = 0 \quad \text{at } \theta = 180^\circ. \tag{59}$$

In addition to the above conditions, all the stress components are continuous along each border of two neighboring sectors. This condition was first given as an assumption in the work of Drugan et al. [24] and was proved later independently by Drugan and Rice [16] and Gao and Hwang [17] for growing cracks. Note that radial stress discontinuity is allowed for assembly of crack-tip sectors for stationary cracks, for example, see Kim and Pan [37] for stationary cracks in pressure-sensitive Drucker–Prager materials. However, the corresponding finite element computational results show no radial stress discontinuity (see more references in Kim and Pan [37] on this issue).

Furthermore, another border condition between the first non-singular sector (sector C) and the elastic sector (sector D) is

$$\dot{\Lambda}(\theta = \theta_3) = 0, \tag{60}$$

where θ_3 is defined in Figure 2. Equation (60) has been proved by Gao and Hwang [17] and used for the assembly of crack-tip fields for elastic perfectly plastic Mises materials by Hwang and Lou [26].

In order to determine the constants of the velocity field in the first non-singular plastic sector (sector C), the continuity conditions of v_r and v_θ were applied along the border between the centered fan sector (sector B) and the non-singular plastic sector (sector C). If the dominant

$\ln(1/r)$ singular terms are considered, the constants of the velocity field can be determined from Equations (18), (19), (45) and (46) as

$$A_1 = -\frac{1}{E}\left[Y(\theta_2)\cos\theta_2 + \sin\theta_2 \int_{\theta_1}^{\theta_2} [Y(\theta) - P_{\theta\theta}X(\theta)]\ \mathrm{d}\theta\right] \tag{61}$$

$$A_2 = -\frac{1}{E}\left[Y(\theta_2)\sin\theta_2 - \cos\theta_2 \int_{\theta_1}^{\theta_2} [Y(\theta) - P_{\theta\theta}X(\theta)]\ \mathrm{d}\theta\right] \tag{62}$$

where $Y(\theta)$ is given in Equation (34) and $X(\theta)$ in Equation (42). Further, sectors C, D, and E have the same form of velocity fields (see Equations (18) and (19) with constants A_1 and A_2 for sector C, A_6 and A_7 for sector D, and A_{12} and A_{13} for sector E, respectively). Therefore, under the assumption of full velocity continuity, all the corresponding constants for the velocity fields in sectors C, D and E are identical: $A_1 = A_6 = A_{12}$ and $A_2 = A_7 = A_{13}$.

The solution procedure is given as follows. Two parameters, the stress component σ_{11} at $\theta = 0$ and the value of θ_2 are first assumed as the initial guesses. In the constant stress sector, the other two stress components σ_{22} and σ_{33} at $\theta = 0$ can be determined by the yield condition and the plane strain conditions for singular plastic sector ($P_{33} = 0$). The value of θ_1 is determined by Kim and Pan [37] as

$$\theta_1 = \tfrac{1}{2}\tan^{-1}\left(\frac{[1 - \frac{4}{3}\mu^2]^{\frac{1}{2}}}{\mu}\right). \tag{63}$$

The condition of full stress continuity is imposed to determine the stresses at $\theta = \theta_1$ on the side of the centered fan sector. In the centered fan sector, the closed-form stress solutions [37] are employed to calculate the stresses from $\theta = \theta_1$ to the initially guessed angle θ_2 . After the stress field in the centered fan sector is found, the two constants A_1 and A_2 for the velocity singularity are calculated by solving $X(\theta)$ and $Y(\theta)$ and performing integrations in Equations (61) and (62). The full stress continuity then gives all the necessary values to start the Runge–Kutta numerical integration of the differential Equations in (52), (53), (56) and (57) for the non-singular plastic sector (sector C) from $\theta = \theta_2$.

Since $P_{33} = P_{rr} = 0$ for the centered fan sector, the ratio P_{rr}/P_{33} in Equations (56) and (57) is undetermined at $\theta = \theta_2$. To start the numerical integration in sector C, we employed the Taylor's series expansion at $\theta = \theta_2$ to obtain the stresses at $\theta = \theta_2 + \delta\theta$, where $\delta\theta$ is a small angle, as in Drugan et al. [24]. A detailed discussion of the Taylor's series expansion at $\theta = \theta_2$ is included in the Appendix. In summary, the Taylor's series expansion from $\theta = \theta_2$ to $\theta = \theta_2 + \delta\theta$ is not unique and should be dependent on the ratio P_{33}/P_{rr} at $\theta = \theta_2$ approached from the side of the non-singular plastic sector. This ratio cannot be determined simply by the continuity of stresses and velocities at $\theta = \theta_2$. However, a non-negative proportionality factor $\dot{\Lambda}$ at $\theta = \theta_2$ requires that the ratio P_{rr}/P_{33} at $\theta = \theta_2$ satisfies

$$-\frac{1}{2}\left(\frac{3 + 2\mu^2}{3 - \mu^2}\right) \leqslant \left(\frac{P_{rr}}{P_{33}}\right)_{\theta=\theta_2} \leqslant -\nu, \tag{64}$$

where

$$(\quad)_{\theta=\theta_2} \equiv \lim_{\theta\to\theta_2}(\quad) \tag{65}$$

and $\theta > \theta_2$. Note that since $\theta > \theta_2$, the limit value in Equation (65) is evaluated by approaching to θ_2 from the side of the non-singular plastic sector. The lower bound

$$\left(\frac{P_{rr}}{P_{33}}\right)_{\theta=\theta_2} = -\frac{1}{2}\left(\frac{3+2\mu^2}{3-\mu^2}\right) \tag{66}$$

in Equation (64) corresponds to a set of solutions where σ'_{ij} are continuous at $\theta = \theta_2$ (see Appendix).

The general expressions of the Taylor's series expansion for P_{33} and P_{rr} are in the form of Equations (A45) and (A46) and the stress components derived from these two equations are found to be rather complicated. Since the variation of the stress fields due to different values of $(P_{33}/P_{rr})_{\theta=\theta_2}$ within the bounds specified by Equation (64) is found to be very small, only the Taylor's series expansions at $\theta = \theta_2$ under the assumption of Equation (66) are shown in the following. Because $(P'_{33})_{\theta=\theta_2} = 0$ under the condition of Equation (66), the Taylor's series expansion for P_{33} and P_{rr} at $\theta = \theta_2 + \delta\theta$ is written as

$$P_{33} = C(\theta-\theta_2)^2 + \cdots \tag{67}$$

$$P_{rr} = -\frac{1}{2}\left(\frac{3+2\mu^2}{3-\mu^2}\right) C(\theta-\theta_2)^2 + \cdots, \tag{68}$$

where $\theta > \theta_2$ and $C = \frac{1}{2}(P''_{33})_{\theta=\theta_2}$. Here C is a constant and again cannot be determined from available boundary conditions at $\theta = \theta_2$. However, to get a non-negative $\dot{\Lambda}$, we need $C \geqslant 0$.

From Equations (52), (53), (67), (68) and the closed-form stress solutions of the centered fan sector, we obtain the Taylor's series expansion of the stresses at $\theta = \theta_2 + \delta\theta$ for $\mu > 0$ as

$$\sigma_{r\theta} = \sigma^0_{r\theta} + \frac{2\mu}{(1-\frac{4}{3}\mu^2)^{1/2}}\sigma^0_{r\theta}(\theta-\theta_2) + \frac{2\mu^2}{1-\frac{4}{3}\mu^2}\sigma^0_{r\theta}(\theta-\theta_2)^2 + \cdots \tag{69}$$

$$\sigma_{\theta\theta} = \sigma^0_{\theta\theta} - 2\sigma^0_{r\theta}(\theta-\theta_2) - \frac{2\mu}{(1-\frac{4}{3}\mu^2)^{1/2}}\sigma^0_{r\theta}(\theta-\theta_2)^2 + \cdots \tag{70}$$

$$\begin{aligned}\sigma_{33} = {} & \frac{(3+2\mu^2)\sigma^0_{\theta\theta} - 2\sqrt{3}\mu}{3-4\mu^2} - \frac{2(3+2\mu^2)\sigma^0_{r\theta}}{3-4\mu^2}(\theta-\theta_2) \\ & - \left\{\frac{2\sqrt{3}\mu(3+2\mu^2)}{(3-4\mu^2)^{3/2}}\sigma^0_{r\theta} + \frac{9(\sqrt{3}\mu\sigma^0_{\theta\theta}-1)}{(3-\mu^2)(3-4\mu^2)}\right\} C(\theta-\theta_2)^2 + \cdots\end{aligned} \tag{71}$$

$$\begin{aligned}\sigma = {} & \frac{(3-\mu^2)\sigma^0_{\theta\theta} - \sqrt{3}\mu}{3-4\mu^2} - \frac{2(3-\mu^2)\sigma^0_{r\theta}}{3-4\mu^2}(\theta-\theta_2) \\ & - \frac{2\sqrt{3}\mu(3-\mu^2)\sigma^0_{r\theta}}{(3-4\mu^2)^{3/2}}(\theta-\theta_2)^2 + \cdots\end{aligned} \tag{72}$$

where $\sigma^0_{r\theta} = \sigma_{r\theta}(\theta = \theta_2)$ and $\sigma^0_{\theta\theta} = \sigma_{\theta\theta}(\theta = \theta_2)$. We have adopted different values of $C(\geqslant 0)$ in our solution procedure and found that the values of C chosen have very weak influences on the stress fields.

The Runge–Kutta integration is then performed from $\theta = \theta_2 + \delta\theta$ with the initial value obtained by the Taylor's series expansion described above. The non-singular plastic sector ends where the zero plastic dissipation condition in Equation (60) is satisfied. The value of θ_3 in Equation (60) is found by checking at the end point of each Runge–Kutta integration started from θ_2 to decide the two end values of the interval where the solution of θ_3 exists. A bisection iteration method is then applied to find θ_3 in this interval in order to satisfy the requirement of Equation (60). Then, the full stress continuity is again enforced at θ_3 to determine the constants A_8, A_9, A_{10} and A_{11} for the elastic stress field in sector D described by Equations (22), (23), (24), and (25).

In order to find θ_4, θ is increased from θ_3 to the interval where the generalized tensile effective stress σ_{ge} at the end point of the integration interval exceeds σ_0. The angle θ_4 is again determined in this interval by the bisection iteration method as explained earlier for determining θ_3. Once the angle θ_4 is found, the stress state in the second non-singular plastic sector (sector E) can be obtained by numerical integration from θ_4 to 180°. Note that one of the governing equations for the non-singular plastic sector, Equation (57), is singular at $\theta = 180^\circ$. Therefore, the Runge–Kutta integration is used to perform integration from $\theta = \theta_4$ to $\theta = 180^\circ - \Delta\theta$ where $\Delta\theta$ is small in the order of the step size of integration. Then, the Euler integration scheme is used to perform integration from $\theta = 180^\circ - \Delta\theta$ to $\theta = 180^\circ$ to avoid the singular behavior of Equation (57) at $\theta = 180^\circ$. Note that it is not necessary to employ Taylor's series expansion at $\theta = 180^\circ$ as we did at $\theta = \theta_2$, although Hwang and Lou [26] did implement a modified boundary condition at $\theta = 180^\circ - \eta$ ($\eta = 0.1^\circ$) by the Taylor's series expansion from the boundary conditions at $\theta = 180^\circ$.

At $\theta = 180^\circ$, the traction-free conditions on the crack surface, $\sigma_{\theta\theta} = \sigma_{r\theta} = 0$ are tested. If these two traction-free boundary conditions are not satisfied, new trial values for σ_{11} and θ_2 are selected by the Newton–Raphson method. The procedure is continued until the traction-free conditions at $\theta = 180^\circ$ are satisfied. In the Runge–Kutta numerical integration scheme for the non-singular plastic sectors, three different increments of the angle (0.01°, 0.001° and 0.0001°) have been used to assess the accuracy of the calculations. All three of them give the almost same results for the angles to the order of 0.1°.

7. Numerical results

First, it should be noted that the value of E/σ_0 has no influence on the stress fields. This can be observed from the governing equations of each sector and the continuity condition of stresses. However, the value of E/σ_0 does affect the velocity constants A_1 ($= A_6 = A_{12}$) and A_2 ($= A_7 = A_{13}$) in Equations (61) and (62). As indicated in Equations (61) and (62), a larger value of E/σ_0 corresponds to smaller values of A_1 and A_2 and therefore lower velocities. Note that $Y(\theta)$ and $X(\theta)$ are scaled by σ_0 in Equations (61) and (62).

To verify our solution procedure, we have obtained the stress fields for Mises materials ($\mu = 0$). The results are compared with those of Drugan et al. [24] and Hwang and Luo [26]. The stress field for $\mu = 0$ and $\nu = 0.3$, which is shown in Figure 3, agrees well with that of Drugan et al. [24] and Hwang and Luo [26]. Our solution for $\mu = 0$ and $\nu = 0.3$ gives $\theta_1 = 45^\circ$, $\theta_2 = 110.3^\circ$, $\theta_3 = 118.3^\circ$ and $\theta_4 = 160.5^\circ$. The value of $\sigma_{\theta\theta}/\sigma_0$ ahead of the crack tip is 2.95, which is lower than 2.97 of the Prandtl field. Sham [25] has found the asymptotic stress field for a quasi-statically growing crack by finite element analysis. The computed stresses of Sham [25] agree very well with the analytical results of Drugan et al. [24] except the out-of-plane stress ahead of the tip. For $\mu = 0.01$ and $\nu = 0.3$, our solution

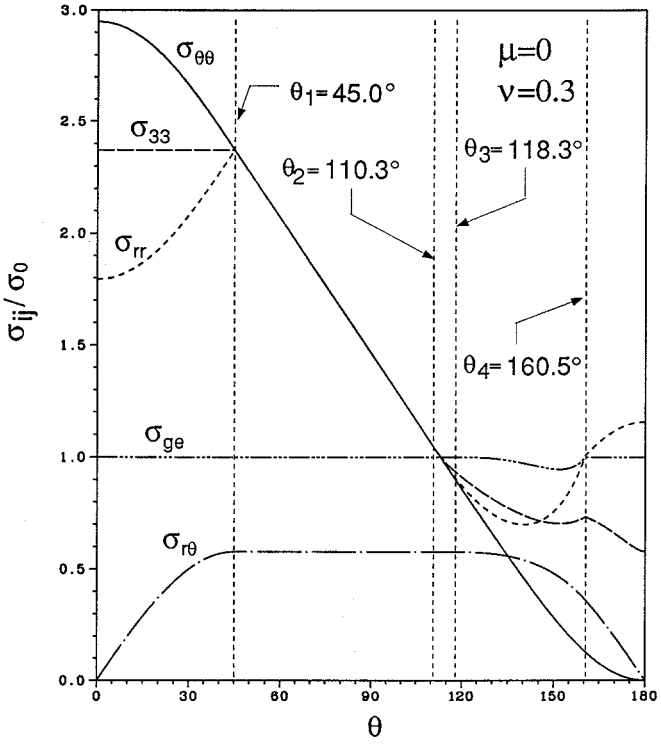

Figure 3. The angular variations of the normalized crack-tip stresses for $\mu = 0$.

gives $\sigma_{\theta\theta}/\sigma_0 = 2.87$ ahead of the crack tip, $\theta_1 = 44.7^\circ$, $\theta_2 = 109.4^\circ$, $\theta_3 = 117.6^\circ$ and $\theta_4 = 160.8^\circ$. The angular distributions of the normalized stresses for $\mu = 0.01$ are quite similar to those of the $\mu = 0$ case and will not be shown here. It has been noticed that there is about a maximum discrepancy of 0.2° between our solutions for θ_2, θ_3, and θ_4 and those of Hwang and Luo [26] for Mises materials for the case of $\nu = 0.3$ and $\nu = 0.4$. The reason is possibly that Hwang and Luo [26] employed an expansion for the boundary conditions from $\theta = 180^\circ$ to $\theta = 180^\circ - \eta$ where η is a small angle ($\approx 0.1^\circ$) and performed numerical integrations to $\theta = 180^\circ - \eta$ [26]. On the other hand, we use the Euler integration scheme with a very small step size for the very last integration step to $\theta = 180^\circ$ to avoid the singular behavior of Equation (57) at $\theta = 180^\circ$.

Figures 4, 5, and 6 show the angular variations of the stress fields for $\mu = 0.2$, 0.4, and 0.6 with $\nu = 0.3$. Results are only shown for μ lower than 0.6 because the angle θ_4 becomes very close to 180° as μ is larger than 0.6. As shown in the figures, when μ increases, the total angular span of the constant stress sector (sector A) and the centered fan sector (sector B) decreases. This trend agrees with that in Kim and Pan [37] for stationary cracks under small-scale yielding with no T stresses. Also, as μ increases, the angular span of the elastic sector (sector D) increases. The angular span of the trailing non-singular sector (sector E), on the other hand, decreases from 19.5° for $\mu = 0$ to 0.4° for $\mu = 0.6$. When μ is larger than 0.6, the angular span of the trailing non-singular plastic sector (sector E) becomes even smaller and almost vanishes.

Note that asymptotic analyses of near-tip fields for growing cracks in pressure-sensitive materials have been presented by Miao and Drugan [38], Bigoni and Radi [30], and Radi

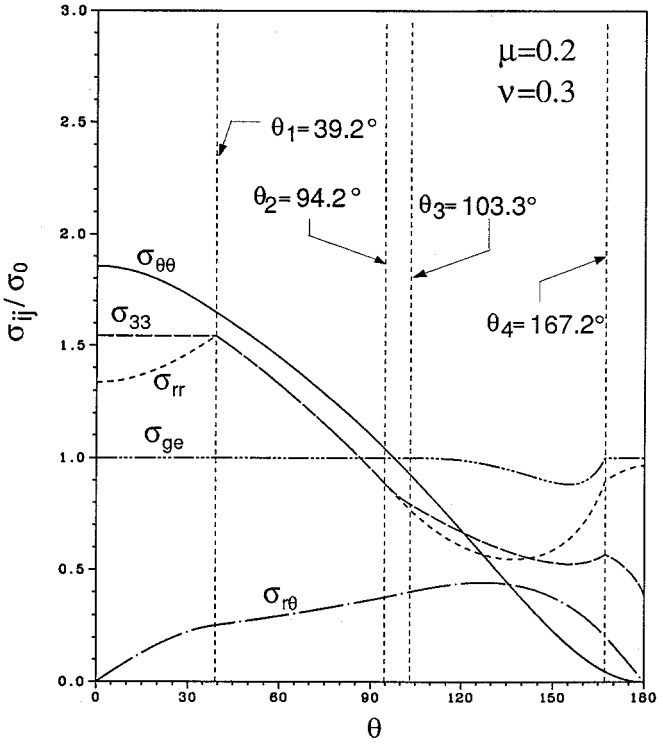

Figure 4. The angular variations of the normalized crack-tip stresses for $\mu = 0.2$.

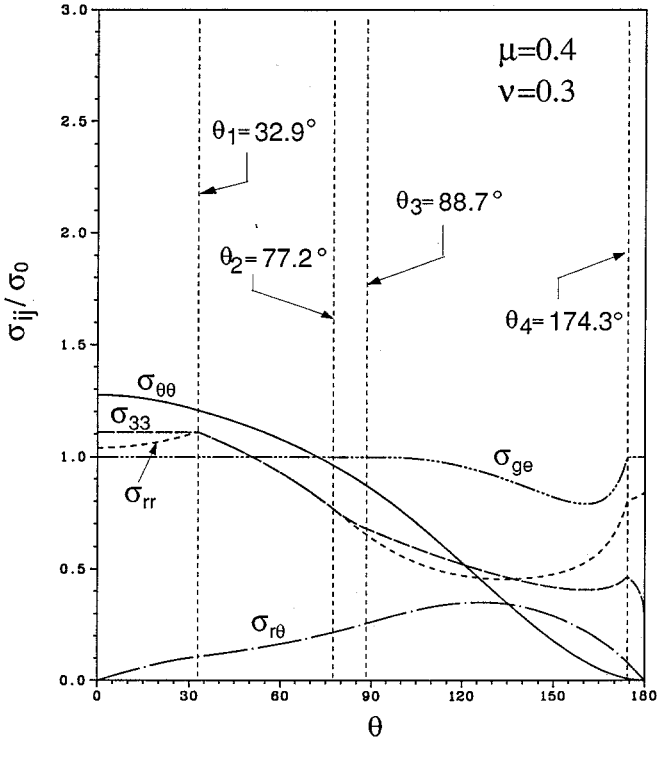

Figure 5. The angular variations of the normalized crack-tip stresses for $\mu = 0.4$.

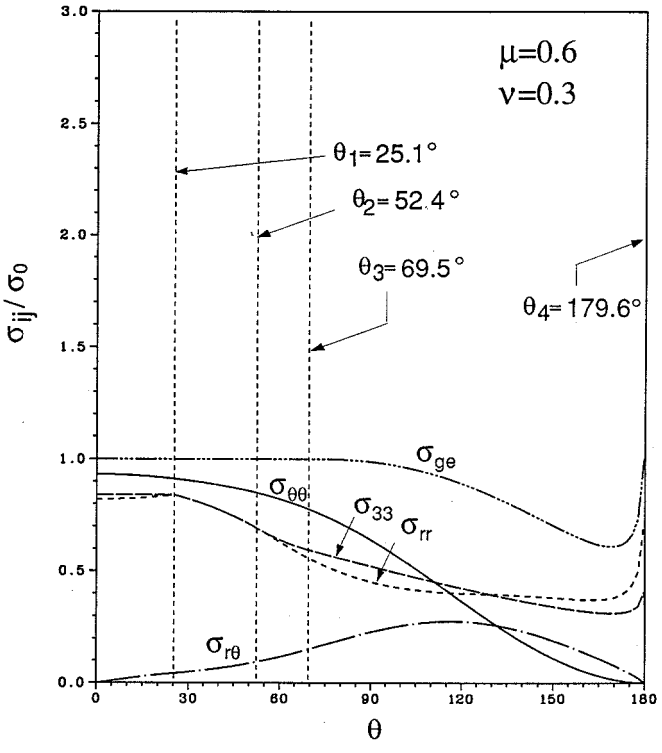

Figure 6. The angular variations of the normalized crack-tip stresses for $\mu = 0.6$.

and Bigoni [39, 40]. Miao and Drugan [38] obtained the plane strain growing crack-tip fields for porous perfectly plastic materials based on Gurson's yield criterion [41]. Radi and Bigoni [39, 40] investigated the growing crack-tip fields for porous linear hardening materials with isotropic hardening and with combined isotropic and kinematic hardening, respectively, based on Gurson's yield criterion. Note that in the above-mentioned asymptotic analyses for porous materials, the void volume fraction was assumed to be independent of r and θ. Also, Bigoni and Radi [30] investigated the plane-strain and plane-stress growing crack-tip fields for linear hardening pressure-sensitive materials based on the Drucker–Prager yield criterion.

As the pressure sensitivity increases, our asymptotic results show (i) a decrease of the total angular span of the plastic sectors in front of the crack tip, (ii) an increase of the angular span of the elastic sector, and (iii) a decrease of the angular span of the plastic reloading sector. Both the solutions of Miao and Drugan [38] for porous perfectly plastic materials and those of Radi and Bigoni [39] for porous isotropic hardening materials show the trends of (i), (ii), and (iii) as the porosity increases. The solutions of Bigoni and Radi [30] for linear hardening Drucker–Prager materials show only the trend of (i) as the pressure sensitivity increases. The solutions of Radi and Bigoni [40] for nearly isotropic hardening materials show the trends of (i), (ii) and (iii) as the porosity increases. However, for nearly kinematic hardening materials, their results [40] show that, for various values of the porosity, the angular span of the plastic loading sector becomes very large, the angular span of the elastic unloading sector becomes very small, and the angular span of the plastic reloading sector becomes very small or disappears, depending upon the hardening.

Table 1. Normalized stresses ahead of the crack tip at $\theta = 0^\circ$ for mode I stationary and growing cracks ($\nu = 0.3$)

	Stationary crack		Growing crack	
μ	σ_{rr}	$\sigma_{\theta\theta}$	σ_{rr}	$\sigma_{\theta\theta}$
0	1.8138	2.9685	1.7941	2.9488
0.2	1.3734	1.8807	1.3360	1.8558
0.4	1.0934	1.2973	1.0387	1.2745
0.6	0.8918	0.9468	0.8197	0.9309

Table 2. Border angles of crack-tip sectors

	θ_1		θ_2		θ_3		θ_4	
μ	$\nu = 0.3$	$\nu = 0.4$	$\nu = 0.3$	$\nu = 0.4$	$\nu = 0.3$	$\nu = 0.4$	$\nu = 0.3$	$\nu = 0.4$
0	45°	45°	110.3°	111.6°	118.3°	113.8°	160.5°	161.7°
0.2	39.2°	39.2°	94.2°	95.4°	103.3°	98.3°	167.2°	168.4°
0.4	32.9°	32.9°	77.2°	78.2°	88.7°	83.4°	174.3°	175.2°
0.6	25.1°	25.1°	52.4°	53.1°	69.5°	63.5°	179.6°	179.8°

The asymptotic solutions of the stresses at $\theta = 0^\circ$ for growing cracks and those for stationary cracks in Li and Pan [9] are listed in Table 1 for $\nu = 0.3$ and $\mu = 0$, 0.2, 0.4, and 0.6. As shown in Table 1, the stresses at $\theta = 0^\circ$ for growing cracks are slightly lower than those for stationary cracks.

Non-negative plastic dissipation is an important concern for the validity of the solution. Negative plastic dissipation is not allowed in the solution. The plastic dissipation in the centered fan sector can be represented in Equation (41). Note that $X(\theta)$ is the coefficient of the most singular term of $\dot{\Lambda}$ in Equation (41). We have checked that $X(\theta)$ is positive throughout the entire sector. Also, we have used Equation (51) to verify the positiveness of $\dot{\Lambda}$ inside the two non-singular plastic sectors. We have not observed any negative plastic dissipation throughout our numerical results of the crack-tip fields.

We have also investigated the effect of Poisson's ratio ν on the crack-tip fields. The angles of the borders between sectors and the angular spans of sectors for $\nu = 0.3$ and 0.4 are listed in Tables 2 and 3. When the results for $\nu = 0.3$ and 0.4 are compared, we can see that the angular span of the centered fan sector (sector B) increases, the angular spans of the two non-singular

Table 3. Angular spans of crack-tip sectors

	Sector A		Sector B		Sector C		Sector D		Sector E	
μ	$\nu = 0.3$	$\nu = 0.4$	$\nu = 0.3$	$\nu = 0.4$	$\nu = 0.3$	$\nu = 0.4$	$\nu = 0.3$	$\nu = 0.4$	$\nu = 0.3$	$\nu = 0.4$
0	45°	45°	65.3°	66.6°	8.0°	2.2°	42.2°	47.9°	19.5°	18.3°
0.2	39.2°	39.2°	55.0°	56.2°	9.1°	2.9°	63.9°	70.1°	12.8°	11.6°
0.4	32.9°	32.9°	44.3°	45.3°	11.5°	5.2°	85.6°	91.8°	5.7°	4.8°
0.6	25.1°	25.1°	27.3°	28.0°	17.1°	10.4°	110.1°	116.3°	0.4°	0.2°

plastic sectors (sector C and sector E) decrease, and the angular span of the elastic sector (sector D) increases as ν increases. Note that the angular span of sector A is not affected by Poisson's ratio ν.

The results of the asymptotic crack-tip fields can be used to formulate a crack growth criterion, as that by Rice et al. [22] and Drugan et al. [24] for Mises materials. The formulation is quite straightforward by following the approach of Rice et al. [22] and Drugan et al. [24]. However, the constants in the crack growth criterion cannot be completely determined by the asymptotic analysis. A finite element analysis of the near-tip fields for pressure-sensitive materials can be used to determine and validate the necessary constants in the crack growth criterion (for example, see Rice et al. [22] and Drugan et al. [24]).

The effects of phase transformation on toughening of zirconia ceramics have been studied by McMeeking and Evans [42], Budiansky et al. [43], and Stump and Budiansky [44] based on a mean stress phase transformation criterion. The effects of shear on transformation toughening have been investigated by Lambropoulos [45] and Stam et al. [46]. It should be noted that for phase transformation ceramics, the phase transformation strains are finite. As the radial distance to the crack tip decreases, the stresses increase and the phase transformation occurs. The material appears to behave plastically. However, as the radial distance to the tip continues to decrease and the phase transformation of the material is completed, the material behaves elastically again. The effects of the second elastic behavior at large strains on the stationary crack-tip fields for strong phase transformation materials are discussed in details in Kim and Pan [37]. From this viewpoint, the nature of asymptotic growing crack-tip fields for phase transformation ceramics is quite different from that of growing crack-tip fields for elastic-plastic materials where the plastic strains can be infinitely large and the elastic behavior usually comes from elastic unloading.

8. Conclusion

Quasi-statically growing crack-tip fields for pressure-sensitive materials under mode I plane strain conditions are studied in this paper. The materials are assumed to follow the Drucker–Prager yield criterion and the normality flow rule. The results of the asymptotic analysis show that as the pressure sensitivity increases, the total angular span (θ_3) of the front plastic sectors decreases, the angular span of the elastic unloading sector increases, and the angular span of the trailing non-singular plastic sector decreases. A finite element analysis of the near-tip fields for growing cracks in pressure-sensitive materials is suggested for development of a crack growth criterion for pressure-sensitive materials.

Acknowledgements

This work was supported by the National Science Foundation Materials Research Group under grant number DMR-8708405.

Appendix A

In this appendix, we will show that the Taylor's series expansions at $\theta = \theta_2$ along the border between the centered fan sector (sector B) and the first non-singular sector (sector C) cannot be fully determined simply by the continuity of stresses at $\theta = \theta_2$ and the governing equations for the non-singular plastic sectors. The Taylor's series expansion at $\theta = \theta_2$ for Mises materials

($\mu = 0$) derived by Drugan et al. [24] is just a special case in which the stresses and derivatives of stresses are assumed to be continuous at $\theta = \theta_2$. A family of the Taylor's series expansions exists such that the discontinuities of the first derivatives of the stress components σ_{rr} and σ_{33} at $\theta = \theta_2$ are allowed and the requirement of non-negative plastic dissipation ($\dot{\Lambda} \geqslant 0$) is satisfied. However, our numerical results show that the crack-tip stress fields do not change significantly when different allowable Taylor's series expansions at $\theta = \theta_2$ are employed. In the following, the Taylor's series expansions at $\theta = \theta_2$ for Mises materials are first investigated because of the availability of the closed-form solutions of the velocity field in the centered fan. Then, a parallel analysis is carried out for pressure-sensitive materials.

A.1. Mises materials

For Mises materials, the governing equations, Equations (52), (53), (56), and (57), for non-singular plastic sectors can be reduced to

$$\sigma'_{r\theta} = 2(\sigma_{\theta\theta} - \sigma) \tag{A1}$$

$$\sigma'_{\theta\theta} = -2\sigma_{r\theta} \tag{A2}$$

$$\sigma' = \frac{2E(A_1 \cos\theta/\sin\theta + A_2)}{4 + 4\nu[2((\sigma - \sigma_{\theta\theta})/s_{33}) - 1] + [2((\sigma - \sigma_{\theta\theta})/s_{33}) - 1]^2} \tag{A3}$$

$$s'_{33} = -\frac{4(\sigma - \sigma_{\theta\theta})\sigma'}{3s_{33}}, \tag{A4}$$

where

$$A_1 = -[(5 - 4\nu/\sqrt{2}](\tau_0/E)\sin\theta_2 \tag{A5}$$

$$A_2 = -[(5 - 4\nu/\sqrt{2}](\tau_0/E)(\sqrt{2} - \cos\theta_2). \tag{A6}$$

and $\tau_0 = \sigma_0/\sqrt{3}$ is the shear yield stress.

The closed-form solutions of the stresses in the centered fan sector are

$$\sigma_{r\theta} = \tau_0 \tag{A7}$$

$$\sigma_{\theta\theta} = C_f - 2\tau_0\theta \tag{A8}$$

$$\sigma = C_f - 2\tau_0\theta \tag{A9}$$

$$s_{33} = 0, \tag{A10}$$

where C_f is a constant depending on the boundary conditions. The stresses σ_{ij} at $\theta = \theta_2$ are continuous. To obtain the Taylor's series expansions of $\sigma_{r\theta}$, $\sigma_{\theta\theta}$, σ, and s_{33} at $\theta = \theta_2$, we need to obtain the derivatives of these four variables evaluated at $\theta = \theta_2$ using Equations (A1)–(A4) and the continuity condition of the stresses at $\theta = \theta_2$. Note that

$$(\sigma - \sigma_{\theta\theta})_{\theta=\theta_2} = (s_{33})_{\theta=\theta_2} = 0, \tag{A11}$$

from Equations (A8)–(A10). Therefore, the ratio $(\sigma - \sigma_{\theta\theta})/s_{33}$ at $\theta = \theta_2$ cannot be determined. Consequently, σ' cannot be determined by Equation (A3) unless the ratio $(\sigma - \sigma_{\theta\theta})/s_{33}$ at $\theta = \theta_2$ is determined.

Here we assume

$$\left(\frac{\sigma-\sigma_{\theta\theta}}{s_{33}}\right)_{\theta=\theta_2}=\gamma. \tag{A12}$$

Note that γ is assumed to be 0 in Drugan et al. [24]. Combining Equations (A3), (A5), (A6), and (A12), we have

$$(\sigma')_{\theta=\theta_2}=\frac{-2(5-4\nu)\tau_0}{4+4\nu(2\gamma-1)+(2\gamma-1)^2}. \tag{A13}$$

After rearranging Equation (A13), we can show that

$$\frac{5-4\nu}{4(1-\nu^2)}(-2\tau_0)\leqslant(\sigma')_{\theta=\theta_2}<0. \tag{A14}$$

This implies that we can obtain a family of the Taylor's series expansions at $\theta=\theta_2$ when no further restrictions are applied to γ.

The proportionality factor $\dot{\Lambda}$ in Equation (51) for non-singular plastic sectors can be rewritten as

$$\dot{\Lambda}=-\frac{\dot{a}\sin\theta}{rEs_{33}}\left\{-\frac{4(\sigma-\sigma_{\theta\theta})}{3s_{33}}+\tfrac{2}{3}(1-2\nu)\right\}\sigma'\geqslant 0 \tag{A15}$$

for Mises materials, with the use of Equation (A4) and $P_{33}=3s_{33}/2$ ($\mu=0$ and $\sigma_e=1$). Note that $\dot{\Lambda}$ must be non-negative. Also note that because $(s_{33})_{\theta=\theta_2}=0$, $\dot{\Lambda}$ is singular at $\theta=\theta_2$ for $\nu<\frac{1}{2}$.

In the following, we will try to find the values of γ that meets the requirement of Equation (A15). We apply the Taylor's series expansion for s_{33} at $\theta=\theta_2$

$$s_{33}=(s_{33})_{\theta=\theta_2}+(s'_{33})_{\theta=\theta_2}(\theta-\theta_2)+\tfrac{1}{2}(s''_{33})_{\theta=\theta_2}(\theta-\theta_2)^2+\cdots, \tag{A16}$$

where $(\quad)_{\theta=\theta_2}$ is defined in Equation (65). Since $(s_{33})_{\theta=\theta_2}=0$, the general form of Equation (A16) can be represented as

$$s_{33}=C_1(\theta-\theta_2)+C_2(\theta-\theta_2)^2+\cdots, \tag{A17}$$

where $C_1=(s'_{33})_{\theta=\theta_2}$, $C_2=(\frac{1}{2})(s''_{33})_{\theta=\theta_2}$, ...

If the derivatives of σ_{ij} with respect to θ, σ'_{ij}, are continuous at $\theta=\theta_2$, we have $(s'_{33})_{\theta=\theta_2}=0$. Therefore, the Taylor's series expansion of s_{33} in Equation (A17) becomes

$$s_{33}=C_2(\theta-\theta_2)^2+\cdots \tag{A18}$$

because $C_1=(s'_{33})_{\theta=\theta_2}=0$. After substituting Equation (A18) into (A4), we obtain

$$\sigma-\sigma_{\theta\theta}=-\frac{3{C_2}^2}{4\sigma'}(\theta-\theta_2)^3+\cdots \tag{A19}$$

From Equations (A18) and (A19), we have

$$\left(\frac{\sigma-\sigma_{\theta\theta}}{s_{33}}\right)_{\theta=\theta_2}=\gamma=0. \tag{A20}$$

To check if Equation (A15) is satisfied near $\theta=\theta_2$ on the side of the non-singular plastic sector, we evaluate the positiveness of $\dot{\Lambda}$ at $\theta=\theta_2+\delta\theta$ (because $\dot{\Lambda}$ is singular at $\theta=\theta_2$),

where $\delta\theta$ is a positive yet infinitesimal angle. Substituting Equations (A18) and (A20) into (A15) with $\nu < 1/2$, we arrive at

$$C_2 \geqslant 0. \tag{A21}$$

Note that we assume

$$(\quad)_{\theta=\theta_2} \approx (\quad)_{\theta=\theta_2+\delta\theta} \tag{A22}$$

in the above derivation. When $\nu = \frac{1}{2}$, no specific constraint condition can be obtained for C_2. However, for Mises materials with $\nu = \frac{1}{2}$, the non-singular plastic sector between the centered fan sector and the elastic sector degenerates to a line in the assembly of the crack-tip field [22, 26]. The Taylor's series expansion for s_{33} therefore is not needed for Mises materials with $\nu = \frac{1}{2}$. So far we have shown that σ'_{ij} can be continuous at $\theta = \theta_2$ without violating Equation (A15). Note that $\gamma = 0$ corresponds to the assumption that σ'_{ij} are continuous at $\theta = \theta_2$.

Next, we assume that some components of σ'_{ij} are allowed to be discontinuous at $\theta = \theta_2$. Since $\sigma'_{r\theta}$ and $\sigma'_{\theta\theta}$ are continuous at $\theta = \theta_2$ from Equations (A1) and (A2) and the continuity of stresses, we are allowing the discontinuity of σ' and s'_{33} (or, σ'_{rr} and σ'_{33}) at $\theta = \theta_2$. In this case, $(s'_{33})_{\theta=\theta_2} \neq 0$. The Taylor's series expansion of s_{33} is represented by Equation (A17). From Equation (A17), we can show that

$$\text{sign}\{(s_{33})_{\theta=\theta_2+\delta\theta}\} = \text{sign}\{(s'_{33})_{\theta=\theta_2+\delta\theta}\}. \tag{A23}$$

Recall that $\delta\theta$ is positive and infinitesimal. From Equation (A4) with $\sigma' < 0$ (see Equation (A14)) and Equation (A23), we can show that

$$(\sigma - \sigma_{\theta\theta})_{\theta=\theta_2+\delta\theta} > 0. \tag{A24}$$

With the use of Equations (A24) and (A15), we can further show that only

$$(s_{33})_{\theta=\theta_2+\delta\theta} > 0 \tag{A25}$$

can satisfy both the condition of $\dot{\Lambda} \geqslant 0$ and Equation (A4). Substituting Equation (A24) and Equation (A25) into Equation (A15) leads to

$$\gamma \leqslant \tfrac{1}{2} - \nu. \tag{A26}$$

Also, from Equation (A24) and Equation (A25) we have

$$\gamma > 0. \tag{A27}$$

Therefore,

$$0 < \gamma \leqslant \tfrac{1}{2} - \nu. \tag{A28}$$

Note that when $\nu = 1/2$, Equation (A28) shows that there is no solution available for γ.

From Equations (A20) and (A28), we can conclude that

$$0 \leqslant \gamma \leqslant \tfrac{1}{2} - \nu. \tag{A29}$$

Substituting Equation (A29) into Equation (A13) gives

$$\frac{5 - 4\nu}{4(1 - \nu^2)}(-2\tau_0) \leqslant (\sigma')_{\theta=\theta_2} \leqslant (-2\tau_0) \tag{A30}$$

The two limits of $(\sigma')_{\theta=\theta_2}$ in Equation (A30) correspond to $\gamma = 0$ and $\gamma = \frac{1}{2} - \nu$, respectively. The factor $(5-4\nu)/[4(1-\nu^2)]$ in Equation (A30) is 1.05 and 1 for $\nu = 0.3$ and 0.5, respectively. According to Equation (A30), the change of σ' allowed at $\theta = \theta_2$ is less than 5% for $\nu = 0.3$. The maximum variation of the angles θ_1, θ_2, θ_3, and θ_4 obtained from our numerical solutions with different values of γ for $\nu = 0.3$ is less than 0.08°.

In summary, the effects of the allowable first-order Taylor's series expansions are quite weak on the crack-tip fields. Numerically, a higher-order expansion can essentially be represented by a first-order expansion just slightly deviated from the state of the continuity of stresses and stress derivatives. Therefore, the higher-order Taylor's series expansion as in Drugan et al. [24] should have even weaker effects on the crack-tip fields. It should be noted again that the first-order Taylor's series expansion must meet the requirement of Equation (A30) and the second-order Taylor's series expansion must meet the requirement of Equation (A21) due to positiveness of plastic dissipation. In fact, the specific second-order Taylor's series expansion of s_{33} in Drugan et al. [24] meets the requirement of Equation (A21).

A.2. Pressure-sensitive materials

For pressure-sensitive materials, a parallel analysis to that for Mises materials is carried out here. The governing equations of the non-singular plastic sector for pressure-sensitive materials are Equations (52), (53), (56), and (57). Also, we have $P_{33} = P_{rr} = 0$ at $\theta = \theta_2$ for the centered fan sector. The ratio P_{rr}/P_{33} at $\theta = \theta_2$ cannot be determined simply by the governing equations of the non-singular plastic sector or the continuity of stresses at $\theta = \theta_2$. Consequently, the values of σ'_{33} and σ' in Equations (56) and (57) cannot be determined at $\theta = \theta_2$. Since we have discussed the Taylor's series expansion for Mises materials ($\mu = 0$) in Appendix A.1, we will focus on the Taylor's series expansion for $\mu > 0$ in the following discussions.

For pressure-sensitive materials, the proportionality factor $\dot{\Lambda}$ in Equation (51) can be written as

$$\dot{\Lambda} = \frac{2\sigma'((P_{rr}/P_{33}) + \nu)}{EP_{33}} \frac{\dot{a}}{r} \sin\theta \geqslant 0. \tag{A31}$$

Note that we do not have closed-form solutions for A_1 and A_2 as for Mises materials. Therefore, we cannot obtain any explicit bounds for σ' as in Equation (A30) for Mises materials. However, the numerical solutions of the centered fan sector for both Mises and pressure-sensitive materials indicate that near $\theta = \theta_2$

$$\sigma' < 0. \tag{A32}$$

With this condition, we here start a parallel analysis to that for Mises materials. With the use of Equations (A31) and (A32) and $\theta_2 < 180^\circ$, we can show that

$$P_{rr} + \nu P_{33} \leqslant 0. \tag{A33}$$

Assume

$$\left(\frac{P_{rr}}{P_{33}}\right)_{\theta=\theta_2} = \alpha. \tag{A34}$$

The Taylor's series expansions of P_{33} and P_{rr} at $\theta = \theta_2$ are written as

$$P_{33} = (P_{33})_{\theta=\theta_2} + (P'_{33})_{\theta=\theta_2}(\theta - \theta_2) + \tfrac{1}{2}(P''_{33})_{\theta=\theta_2}(\theta - \theta_2)^2 + \cdots \tag{A35}$$

$$P_{rr} = (P_{rr})_{\theta=\theta_2} + (P'_{rr})_{\theta=\theta_2}(\theta - \theta_2) + \tfrac{1}{2}(P''_{rr})_{\theta=\theta_2}(\theta - \theta_2)^2 + \cdots \tag{A36}$$

Also, we can express P_{33} in terms of σ and σ_{33} as

$$P_{33} = \frac{\sigma_{33} - \sigma}{1 - \mu(2\sigma + \sigma_{33})/\sqrt{3}} + \frac{\mu}{\sqrt{3}}. \tag{A37}$$

Differentiating Equation (A37) with respect to θ with the condition of $P_{33} = 0$ at $\theta = \theta_2$ gives

$$\sigma'_{33} = \frac{3 + 2\mu^2}{3 - \mu^2}\sigma' + \frac{\sigma_e}{1 - \mu^2/3}P'_{33}, \tag{A38}$$

where the effective stress σ_e $(= 1 - \mu(2\sigma + \sigma_{33})/\sqrt{3})$ must be larger than or equal to 0. Equation (A38) will be useful for our later discussions.

If σ'_{ij} are continuous at $\theta = \theta_2$ so that $(P'_{33})_{\theta=\theta_2} = (P'_{rr})_{\theta=\theta_2} = 0$, the Taylor's series expansions of P_{33} and P_{rr} can be represented as

$$P_{33} = C_2(\theta - \theta_2)^2 + \cdots \tag{A39}$$

$$P_{rr} = \alpha C_2(\theta - \theta_2)^2 + \cdots \tag{A40}$$

with the use of Equation (A35), (A36), and (A34), where $C_2 = (\frac{1}{2})(P''_{33})_{\theta=\theta_2}$. From Equation (A38) with $P'_{33} = 0$, we can show that

$$\sigma'_{33} = \frac{3 + 2\mu^2}{3 - \mu^2}\sigma' \tag{A41}$$

at $\theta = \theta_2$. Substituting Equation (A41) into (56) gives

$$\left(\frac{P_{rr}}{P_{33}}\right)_{\theta=\theta_2} = \alpha = -\frac{1}{2}\left(\frac{3 + 2\mu^2}{3 - \mu^2}\right). \tag{A42}$$

Substituting Equations (A42) and (A39) into (A33), we arrive at

$$C_2(\alpha + \nu) \leqslant 0. \tag{A43}$$

Since $\nu \leqslant \frac{1}{2}$ and $\alpha < -\frac{1}{2}$ from Equation (A42) with $\mu > 0$, we have $\alpha + \nu < 0$. Therefore,

$$C_2 \geqslant 0. \tag{A44}$$

Thus, σ'_{ij} may be continuous without violating the requirement of non-negative $\dot{\Lambda}$. In this case, the value of α is represented in Equation (A42) and Equation (A44) has to be satisfied.

If the components of σ'_{ij}, σ'_{rr} and σ'_{33}, are allowed to be discontinuous at $\theta = \theta_2$, we can write the Taylor's series expansions of P_{rr} and P_{33} in Equations (A35) and (A36) as

$$P_{33} = C_1(\theta - \theta_2) + \cdots \tag{A45}$$

$$P_{rr} = \alpha C_1(\theta - \theta_2) + \cdots \tag{A46}$$

where $C_1 = (P'_{33})_{\theta=\theta_2} \neq 0$. Substituting Equations (A45) and (A46) into Equation (A33) leads to

$$C_1(\alpha + \nu) \leqslant 0. \tag{A47}$$

There are two possibilities for C_1: either $C_1 > 0$ or $C_1 < 0$. However, the following derivation shows that $C_1 < 0$ cannot be true. Now, if $C_1 < 0$, from Equation (A38) with $\sigma_e \geqslant 0$ and (56) we can conclude that

$$\alpha \leqslant -\frac{1}{2}\left(\frac{3+2\mu^2}{3-\mu^2}\right). \tag{A48}$$

With $0 < \mu < \sqrt{3}$ and $\nu \leqslant 1/2$, we have

$$\alpha \leqslant -\frac{1}{2}\left(\frac{3+2\mu^2}{3-\mu^2}\right) < -\tfrac{1}{2} \leqslant -\nu. \tag{A49}$$

Equation (A49) leads to $\alpha + \nu < 0$. With $\alpha + \nu < 0$ and $C_1 < 0$, Equation (A47) is violated. Therefore, we must have $C_1 > 0$. From Equation (A47), we then have

$$\alpha \leqslant -\nu. \tag{A50}$$

Note that Equation (A50) gives the upper limit of α.

Next, the lower limit of α is examined. From Equation (A38) with $P'_{33} = C_1 > 0$ and $\sigma_e \geqslant 0$, we can immediately get

$$\frac{\sigma'_{33}}{\sigma'} \leqslant \frac{3+2\mu^2}{3-\mu^2}. \tag{A51}$$

Applying Equation (A51) to Equation (56), we have

$$\left(\frac{P_{rr}}{P_{33}}\right)_{\theta=\theta_2} = \alpha \geqslant -\frac{1}{2}\left(\frac{3+2\mu^2}{3-\mu^2}\right). \tag{A52}$$

Combining Equations (A50) and (A52), we have

$$-\frac{1}{2}\left(\frac{3+2\mu^2}{3-\mu^2}\right) \leqslant \alpha \leqslant -\nu. \tag{A53}$$

For Mises materials ($\mu = 0$), we have $\alpha = \gamma - \frac{1}{2}$ where α is defined in Equation (A34) and γ is defined in Equation (A12). Equation (A53) reduces to Equation (A29) for Mises materials. The effects of the allowable first-order Taylor's series expansions are quite weak on the crack-tip fields as for Mises materials. For example, for $\mu = 0.6$ and $\nu = 0.3$, the maximum allowable variation of σ' is 13% from Equation (A53) and (57). For this case, the maximum variation of the angles θ_1, θ_2, θ_3, and θ_4 obtained from our numerical solutions with different values of α is less than 0.03°. As mentioned earlier for Mises materials, an allowable higher-order Taylor's series expansion can be represented by an allowable first-order Taylor's series expansion from the numerical viewpoint. Therefore, the effects of the allowable higher-order Taylor's series expansion on the crack-tip fields should be even weaker. However, for completeness of presentation, we list the allowable second-order Taylor's series expansions in Equations (69)–(72).

References

1. S.S. Sternstein and L. Ongchin, Yield criteria for plastic deformation of glassy high polymers in general stress fields. *American Chemical Society, Polymer Preprints* 10 (1969) 1117–1124.
2. D.C. Drucker, Plasticity theory, strength-differential (SD) phenomenon, and volume expansion in metals and plastics. *Metallurgical Transactions* 4 (1973) 667–673.
3. W.A. Spitzig and O. Richmond, Effect of hydrostatic pressure on the deformation behavior of polyethylene and polycarbonate in tension and in compression. *Polymer Engineering and Science* 19 (1979) 1129–1139.
4. L.M. Carapellucci and A.F. Yee, The biaxial deformation and yield behavior of Bisphenol-A polycarbonate: Effect of anisotropy. *Polymer Engineering and Science* 26 (1986) 920–930.
5. I.-W. Chen and P.E. Reyes Morel, Implications of transformation plasticity in ZrO_2-containing ceramics: I, shear and dilatation effects. *Journal of the American Ceramic Society* 69 (1986) 181–189.
6. P.E. Reyes-Morel and I.-W. Chen, Transformation plasticity of CeO_2-stabilized tetragonal zirconia polycrystals: I, stress assistance and autocatalysis. *Journal of the American Ceramic Society* 71 (1988) 343–353.
7. C.-S. Yu and D.K. Shetty, Transformation zone shape, size, and crack-growth-resistance (R-curve) behavior of ceria-partially-stabilized zirconia polycrystals. *Journal of the American Ceramic Society* 72 (1989) 921–928.
8. D.C. Drucker and W. Prager, Soil mechanics and plastic analysis or limit design. *Quarterly of Applied Mathematics* 10 (1952) 157–165.
9. F.Z. Li and J. Pan, Plane-strain crack-tip fields for pressure-sensitive dilatant materials. *Journal of Applied Mechanics* 57 (1990) 40–49.
10. F.Z. Li and J. Pan, Plane-stress crack-tip fields for pressure-sensitive dilatant materials. *Engineering Fracture Mechanics* 35 (1990) 1105–1116.
11. J.W. Hutchinson, Singular behaviour at the end of a tensile crack in a hardening material. *Journal of the Mechanics and Physics of Solids* 16 (1968) 13–31.
12. J.W. Hutchinson, Plastic stress and strain fields at a crack tip. *Journal of the Mechanics and Physics of Solids* 16 (1968) 337–347.
13. J.R. Rice and G.F. Rosengren, Plane strain deformation near a crack tip in a power-law hardening material. *Journal of the Mechanics and Physics of Solids* 16 (1968) 1–12.
14. H. Yuan and G. Lin, Elastoplastic crack analysis for pressure-sensitive dilatant materials – Part I: Higher-order solutions and two-parameter characterization. *International Journal of Fracture* 61 (1993) 295–330.
15. H. Yuan, Elastoplastic crack analysis for pressure-sensitive dilatant materials – Part II: Interface cracks. *International Journal of Fracture* 69 (1995) 167–187.
16. W.J. Drugan and J.R. Rice, Restrictions on quasi-statically moving surfaces of strong discontinuity in elastic-plastic solids. In G.J. Dvorak and R.T. Shield (eds), *Mechanics of Material Behavior: The D.C. Drucker Anniversary Volume*. Elsevier Science Publishers, Amsterdam (1984) pp. 59–73.
17. Y.-C. Gao and K.-C. Hwang, On the formulation of plane strain problems for elastic perfectly-plastic medium. *International Journal of Engineering Science* 21 (1985) 765–780.
18. W.J. Drugan, On the asymptotic continuum analysis of quasistatic elastic-plastic crack growth and related problems. *Journal of Applied Mechanics* 52 (1985) 601–605.
19. W.J. Drugan, A more direct and general analysis of moving strong discontinuity surfaces in quasi-statically deforming elastic-plastic solids. *Journal of Applied Mechanics* 53 (1986) 224–226.
20. L.I. Slepyan, Growing crack during plane deformation of an elastic-plastic body. *Izvestiia Akademii nauk SSSR. Mekhanika Tverdogo Tela* 9 (1974) 57–67.
21. Y.-C. Gao, Elastic-plastic field at the tip of a crack growing steadily in perfectly plastic medium (in Chinese). *Acta Mechanica Sinica* 1 (1980) 48–56.
22. J.R. Rice, W.J. Drugan and T.-L. Sham, Elastic plastic analysis of growing cracks. *Fracture Mechanics: Twelfth Conference, ASTM STP 700*. American Society for Testing and Materials (1980) pp. 189–221.
23. J.R. Rice, Elastic-plastic crack growth. In H.G. Hopkins and M.J. Sewell (eds), *Mechanics of Solids: The R. Hill 60th Anniversary Volume*. Pergamon Press, Oxford (1982) pp. 539–562.
24. W.J. Drugan, J.R. Rice and T.-L. Sham, Asymptotic analysis of growing plane strain tensile cracks in elastic-ideally plastic solids. *Journal of the Mechanics and Physics of Solids* 30 (1982) 447–473.
25. T.-L. Sham, A finite-element study of the asymptotic near-tip fields for mode I plane-strain cracks growing stably in elastic-ideally plastic solids. In C.F. Shih and J.P. Gudas (eds), *Elastic Plastic Fracture: Second Symposium, Volume I – Inelastic Crack Analysis, ASTM STP 803*. American Society for Testing and Materials (1983) pp. 52–79.
26. K.C. Hwang and X.F. Luo, Near-tip fields of growing cracks and resistance curves. *Mechanics of Materials* 7 (1989) 271–278.
27. W.J. Drugan and X.-Y. Chen, Plane strain elastic-ideally plastic crack fields for mode I quasistatic growth at large-scale yielding – I. A new family of analytical solutions. *Journal of the Mechanics and Physics of Solids* 37 (1989) 1–26.

28. X.-Y. Chen and W.J. Drugan, Plane strain elastic-ideally plastic crack fields for mode I quasistatic growth at large-scale yielding – II. Global analytical solutions for finite geometries. *Journal of the Mechanics and Physics of Solids* 39 (1991) 895–925.
29. P. Ponte Castañeda, Asymptotic fields in steady crack growth with linear strain-hardening. *Journal of the Mechanics and Physics of Solids* 35 (1987) 227–268.
30. D. Bigoni and E. Radi, Mode I crack propagation in elastic-plastic pressure-sensitive materials. *International Journal of Solids and Structures* 30 (1993) 899–919.
31. W.A. Spitzig, R.J. Sober, and O. Richmond, Pressure dependence of yielding and associated volume expansion in tempered martensite. *Acta Metallurgica* 23 (1975) 885–893.
32. W.A. Spitzig, R.J. Sober and O. Richmond, The effect of hydrostatic pressure on the deformation behavior of maraging and HY-80 steels and its implications for plasticity theory. *Metallurgical Transactions* 7A (1976) 1703–1710.
33. A.J. Kinloch, and R.J. Young, *Fracture Behaviour of Polymers*. Elsevier Applied Science, London and New York (1983).
34. I.-W. Chen, Model of transformation toughening in brittle materials. *Journal of the American Ceramic Society* 74 (1991) 2564–2572.
35. J.W. Rudnicki and J.R. Rice, Conditions for the localization of deformation in pressure-sensitive dilatant materials. *Journal of the Mechanics and Physics of Solids* 23 (1975) 371–394.
36. A. Needleman and J.R. Rice, Limits to ductility set by plastic flow localization. In D.P. Koistinen and N.-M. Wang (eds.), *Mechanics of Sheet Metal Forming*. Plenum Publishing Corporation (1978) pp. 237–265.
37. M. Kim and J. Pan, Effects of non-singular stresses on crack-tip fields for pressure-sensitive materials, Part 1: plane strain case. *International Journal of Fracture* 68 (1994) 1–34.
38. Y. Miao and W.J. Drugan, Asymptotic analysis of growing crack stress/deformation fields in porous ductile metals and implications for stable crack growth. *International Journal of Fracture* 72 (1995) 69–96.
39. E. Radi and D. Bigoni, Crack propagation in porous hardening metals. *International Journal of Plasticity* 10 (1994) 761–793.
40. E. Radi and D. Bigoni, Effects of anisotropic hardening on crack propagation in porous-ductile materials. *Journal of the Mechanics and Physics of Solids* 44 (1996) 1475–1508.
41. A.L. Gurson, Continuum theory of ductile rupture by void growth: Part I – Yield criteria and flow rules for porous ductile media. *Journal of Engineering Materials and Technology* 99 (1977) 2–15.
42. R.M. McMeeking and A.G. Evans, Mechanics of transformation-toughening in brittle materials. *Journal of the American Ceramic Society* 65 (1982) 242–246.
43. B. Budiansky, J.W. Hutchinson and J.C. Lambropoulos, Continuum theory of dilatant transformation toughening in ceramics. *International Journal of Solids and Structures* 19 (1983) 337–355.
44. D.M. Stump and B. Budiansky, Crack-growth resistance in transformation-toughened ceramics. *International Journal of Solids and Structures* 25 (1989) 635–646.
45. J.C. Lambropoulos, Shear, shape and orientation effects in transformation toughening. *International Journal of Solids and Structures* 22 (1986) 1083–1106.
46. G.Th.M. Stam, E. Van der Giessen and P. Meijers, Effect of transformation-induced shear strains on crack growth in zirconia-containing ceramics. *International Journal of Solids and Structures* 31 (1994) 1923–1948.